

How does Graph Structure Modulate Membership-Inference Risk for Graph Neural Networks?

Megha Khosla

Intelligent Systems Department

Delft University of Technology

Delft, The Netherlands

m.khosla@tudelft.nl

Abstract—Graph neural networks (GNNs) have become the standard tool for encoding data and their complex relationships into continuous representations, improving prediction accuracy in several machine learning tasks like node classification, link prediction etc. However, their use in sensitive applications has raised concerns about the potential leakage of training data. Research on privacy leakage in GNNs has largely been shaped by findings from non-graph domains, such as images and tabular data. We emphasize the need of graph specific analysis and investigate the impact of graph structure on node level membership inference. We formalize MI over node–neighbourhood tuples and investigate two important dimensions: (i) training–graph construction and (ii) inference-time edge access. Empirically, snowball’s coverage bias often harms generalisation relative to random sampling, while enabling inter-train–test edges at inference improves test accuracy, shrinks the train–test gap, and yields the *lowest* membership advantage across most of the models and datasets. We further show that the generalisation gap empirically measured as the performance difference between the train and test nodes is an *incomplete* proxy for MI risk: access to edges dominates—MI can rise or fall independent of gap changes. Finally, we examine the auditability of differentially private GNNs, adapting the definition of statistical exchangeability of train–test data points for graph based models. We show that for node level tasks the inductive splits (random or snowball sampled) break exchangeability, limiting the applicability of standard bounds for membership advantage of differential private models.

Index Terms—Membership-inference, Graph Neural Networks

I. INTRODUCTION

Graph Neural Networks (GNNs) have become the de-facto standard for learning on relational data, delivering state-of-the-art results in chemistry, recommender systems, knowledge graphs, and more [1]–[3]. However on the downside, GNNs have been shown to leak private information about the very graphs they are trained on [4]–[12]. Existing privacy risk studies for GNNs mainly adapt techniques from the i.i.d. scenario of images [13], treating each example as independent and largely ignoring the graph structure that binds data points together.

We focus on *membership inference* risk: given access to a trained model, an adversary aims to determine whether a specific data instance was included in its training set. In graph

based machine learning using graph neural networks, what is considered as a *data instance* depends on the task: node-level tasks view each node as an instance (e.g., predicting a protein’s function in a PPI network), edge-level tasks treat each edge as an instance (e.g., recommending a friendship), and graph-level tasks consider the entire graph as a single instance (e.g., classifying a molecule’s toxicity). Our study focuses on the node-level cases, where those instances are inherently interdependent due to the existence of edges between them. This inter-instance dependency is largely absent from prior privacy analyses and leads us to ask: *How strongly does the amount of edge information available during training and at inference modulate node-level membership-inference risk?*

To investigate this question, we start from the inductive setting of [12], where training and test node sets are disjoint and, during training, neither test nodes nor any train–test edges are available. A common way to instantiate such splits is to sample train/test nodes uniformly at random and use the induced subgraphs; while this preserves independence among sampled nodes, it is often unrealistic as random node sampling can result in isolated nodes if none of their neighbours are included, undermining the rationale for graph-based learning.

A more plausible training paradigm is *edge-guided* sampling. Analogous to a web crawler that follows hyperlinks, we adopt *snowball sampling*: starting from seeds, we iteratively add a fixed number of randomly chosen neighbours until the desired training size is reached. This produces a well-connected training graph but is inherently *coverage-biased* in which expansions tend to remain within a few regions, oversampling high-degree hubs while leaving peripheral or distinct communities under-represented. The resulting training distribution is therefore non-i.i.d. with respect to the full graph, motivating our first axis of inquiry: *how does such biased coverage affect generalisation to held-out nodes and, in turn, membership-inference (MI) risk?*

A natural second, graph-specific axis is *edge access at inference*. In our node–neighbourhood formulation, each query supplies a subgraph, and a GNN’s prediction for the given node depends on that subgraph at query time. Even with a fixed train–test node split, adding or withholding edges can

substantially alter the outputs of a frozen model. Unlike i.i.d. domains, an adversary may legitimately provide relational context when probing membership. We therefore ask: *how does the adversary’s edge knowledge modulate MI success?*

Thirdly, MI success is often linked to overfitting and generalisation error [14]. Because the true data-generating distribution is unknown, practitioners use the empirical train–test *gap* as a surrogate. Yet prior work suggests that attacker performance does not always increase with this empirical gap in graph settings [12]. Here, the gap itself depends not only on which nodes are selected for train/test but also on which neighbourhoods are presented at inference. This leads to our third guiding question: *what is the relationship between the generalisation gap and membership inference risk across training-graph constructions (random vs. snowball) and inference-time edge regimes?*

Finally, we study the *theoretical* implications of graph sampling and edge structure on bounding membership advantage (MA) for differentially private models. We adapt the definition of *statistical exchangeability* from [15] to GNNs by treating each example as a node and neighbourhood tuple and show that inductive train/test constructions, whether by random node sampling or snowball sampling, break exchangeability because neighbourhoods are restricted to, and dependent on, the sampled training subgraph. Consequently, the standard MA bounds are *not* reliable auditing surrogates in these regimes. We identify conditions under which exchangeability can hold, clarifying when DP-based MA bounds are auditable and when empirical MI evaluation is necessary.

Next, we introduce the GNN architectures used in our experiments and then provide a brief overview of membership-inference attacks and defenses for GNNs to contextualize our study.

II. BACKGROUND AND RELATED WORK

We begin with a brief overview of graph neural networks which will serve as target or victim models in this work. Specifically, to demonstrate the effect of graph structure on effectiveness of MI attack, we employ three types of GNNs which differ in strategies to aggregate information from the node’s neighborhood towards learning its representation.

A. Graph Neural Networks

Graph Neural Networks (GNNs) are a class of machine learning models designed specifically to learn on graph-structured data. The typical input to a GNN consists of two elements: (\mathbf{X}, \mathbf{A}) . Here, $\mathbf{X} = (\mathbf{x}_1^\top, \mathbf{x}_2^\top, \dots, \mathbf{x}_n^\top)$ represents the feature matrix for the nodes in the graph where \mathbf{x}_i is the input feature vector for node i . The adjacency matrix is represented by $\mathbf{A} \in \mathbb{R}^{n \times n}$ which encodes the connectivity between nodes.

The core operation in GNNs is graph convolution, where each node’s representation is updated by aggregating its own features along with the features of its neighbors. After this aggregation step, the node’s representation is transformed using a non-linear function. More formally, let $\mathbf{x}_i^{(\ell)}$ denote the feature representation of node i at layer ℓ , and let \mathcal{N}_i be

the set of nodes in the 1-hop neighborhood of node i . The graph convolution operation at layer ℓ is defined as follows:

$$\mathbf{z}_i^{(\ell)} = \text{AGGREGATION}^{(\ell)} \left(\left\{ \mathbf{x}_i^{(\ell-1)}, \left\{ \mathbf{x}_j^{(\ell-1)} \mid j \in \mathcal{N}_i \right\} \right\} \right) \quad (1)$$

$$\mathbf{x}_i^{(\ell)} = \text{TRANSFORMATION}^{(\ell)} \left(\mathbf{z}_i^{(\ell)} \right) \quad (2)$$

At the final layer (denoted L), a softmax function is applied to the node representations to produce the predicted class probabilities for each node. This can be expressed as:

$$\mathbf{y}_i \leftarrow \text{softmax}(\mathbf{z}_i^{(L)} \Theta), \quad (3)$$

Here, $\mathbf{y}_i \in \mathbb{R}^c$, where c is the number of classes, and Θ is a learnable weight matrix. The j th element \mathbf{y}_i represents the predicted probability that node i belongs to class j . The above described process enables GNNs to capture the structure of the graph and make predictions based on both node features and the relationships between nodes.

a) Aggregation operations in GNNs: To support our claims throughout this work, we focus on three key aggregation operations in GNNs, which serve as the foundation for more complex aggregation methods. The first aggregation operation is based on the Graph Convolutional Network (GCN) model proposed by [16]. In this model, each node’s representation is updated at each layer by computing a weighted average of its own features and those of its neighbors. Let \mathbf{d} be the graph degree vector obtained after adding self loops to all nodes. The i th element \mathbf{d}_i denotes the degree of node i . The aggregation operation in GCN is then given as

$$\mathbf{z}_i^{(\ell)} \leftarrow \mathbf{W}^{(\ell)} \sum_{j \in \mathcal{N}(i) \cup i} \frac{1}{\sqrt{\mathbf{d}_i \mathbf{d}_j}} \mathbf{x}_j^{(\ell-1)}. \quad (4)$$

Here $\mathbf{W}^{(\ell)}$ is the projection matrix corresponding to layer ℓ . Unlike GCN, GRAPH SAGE [17] explicitly differentiates between the representation of the query node (referred to as the ego node) and that of its neighbors. In GRAPH SAGE, aggregation is performed by concatenating the ego node’s representation with the aggregated representations of its neighbors. Several methods for neighbor aggregation are proposed; in this work, we adopt the mean aggregation method, which computes the average of the neighbors’ representations. After applying the projection operation, the simplified aggregation in GRAPH SAGE can be expressed as follows:

$$\mathbf{z}^{(\ell)} = \mathbf{W}_1^{(\ell)} \mathbf{x}_i^{(\ell-1)} + \mathbf{W}_2^{(\ell)} \cdot \frac{1}{|\mathcal{N}(i)|} \sum_{j \in \mathcal{N}(i)} \mathbf{x}_j^{(\ell-1)} \quad (5)$$

GAT [18] introduces attention weights over the edges to perform the aggregation operation as follows.

$$\mathbf{z}_i^{(\ell,p)} = \sum_{j \in \mathcal{N}(i) \cup i} \alpha_{i,j}^{(p)} \mathbf{W}^{(\ell,p)} \mathbf{x}_j^{(\ell-1)}, \quad (6)$$

where the attention coefficients $\alpha_{i,j}^{(p)} : (\mathbf{x}_i, \mathbf{x}_j) \rightarrow \mathbb{R}$ can be seen as the importance weights for aggregation over edge

(i, j) and computed as in [18]. In the transformation set the P representations corresponding to P attention mechanisms are concatenated after a non-linear transformation to obtain a single representation at layer ℓ .

$$\mathbf{x}_i^{(\ell)} = \left| \left| \left| \begin{array}{l} p=1 \end{array} \right| \right| \right. \text{ReLU} \left(\mathbf{z}_i^{(\ell,p)} \mathbf{W}^{(p\ell)} \right). \quad (7)$$

In this work we only experiment with the above representative aggregation types and do not account for other differences in these methods. For example, GRAPHsAGE was proposed to improve scalability in GNN training in which neighborhood sampling was used to reduce the size of the computational graph. In our implementation we restrict to only vary the aggregation types and the provided neighborhood of the input query node is completely used.

B. Membership inference attacks and defenses

Membership inference (MI) is a fundamental privacy risk for machine learning: black-box and white-box attacks exploit systematic differences in a model's behavior on training (member) vs. held-out (non-member) data [13]–[15], [19]–[21]. Recent work extends MI to graph neural networks (GNNs) by defining the *instance* at the node, edge, or graph level and tailoring the attack surface accordingly [6], [8]–[12]. Typical node-level attacks query a trained GNN with a target node (and optionally its neighborhood), using confidence scores, losses, or shadow-model posteriors as membership signals; threat models vary in (i) access to outputs/parameters and (ii) the relational context included with the query (features only vs. features+edges).

Despite this progress, the use of *relational structure* that distinguishes GNNs from i.i.d. models has not been examined systematically as a driver of MI risk. In particular, prior attacks typically treat the graph as a fixed backdrop and do not analyze how training graph construction and inference time edge access modulates attack success.

To defend against information leaks via membership inference with theoretical guarantees, *differential privacy* (DP) [22] has emerged as the most widely used formalism: it guarantees that the presence or absence of any single data point has only a limited effect on a mechanism's output, thereby constraining an adversary's ability to infer membership. Existing methods for privacy preserving training of GNNs in centralised setting can be grouped into three main classes: (i) knowledge distillation based [23] in which the model trained on private data is never released but is used to train a public model under a weak supervision setting [24], (ii) gradient perturbation techniques in which typically DP-SGD [25] is extended for the case of graphs [26], and (iii) aggregation perturbation where the key idea is to add noise to the aggregate information obtained from the GNN neighborhood aggregation step [27], [28].

In i.i.d. domains, membership–inference (MI) attacks are widely used to *audit* differentially private (DP) learning by providing empirical lower bounds on leakage [14], [15], [29], [30]. While it may seem that these auditing algorithms carry over directly to graphs, we show this intuition can be misleading. We make the assumptions explicit and provide

theoretical support for how train graph construction strategies and inference time edge access affect the validity of these audits.

We next formalize the membership–inference game at the node level, specifying the data distribution, adversary capabilities, and evaluation protocol.

III. NODE-LEVEL MEMBERSHIP INFERENCE

To formalise the node level membership inference attack we will need the following definition for an input to a GNN.

Definition 1 (Joint Distribution \mathcal{D} over Node Tuples). *Let \mathcal{D} denote the distribution over tuples*

$$z_v^{\mathcal{G}_S} := (\mathbf{x}_v, y_v, \mathcal{N}_{\text{strategy}}^L(v), \{\mathbf{x}_u : u \in \mathcal{N}_{\text{strategy}}^L(v)\}),$$

where $\mathbf{x}_v \in \mathbb{R}^d$ is the feature vector of node v , $y_v \in \mathcal{Y}$ is its label, $\mathcal{G}_S = (\mathcal{V}_S, \mathcal{E}_S) \sim \mathcal{S}(\mathcal{G}, n)$ is a subgraph of the full graph \mathcal{G} sampled using a sampling scheme \mathcal{S} , $\mathcal{N}_{\text{strategy}}^L(v)$ is the L -hop neighborhood of v , computed according to a neighborhood selection strategy (e.g., induced neighborhood, sampled neighbors, full graph).

We define node-level membership inference experiment while making explicit the construction of input data instance to the GNN in Experiment 1.

Experiment 1. (Node-Level Membership Inference $\text{Exp}(\mathcal{A}, \Phi, n, \mathcal{S})$) *Let \mathcal{A} be an adversary, Φ a learning algorithm, $n \in \mathbb{N}$ a sample size, and \mathcal{S} a sampling scheme to build train graph. The membership inference experiment proceeds as follows:*

- 1) *Sample a subgraph $\mathcal{G}_S = (\mathcal{V}_S, \mathcal{E}_S) \sim \mathcal{S}(\mathcal{G}, n)$ from the full graph \mathcal{G} .*
- 2) *Train a GNN $\Phi_S = \Phi(\mathbf{X}_S, \mathcal{G}_S)$ using algorithm Φ on the subgraph \mathcal{G}_S .*
- 3) *Choose a bit $b \leftarrow \{0, 1\}$ uniformly at random.*
- 4) *If $b = 0$, sample a member node $v \sim \mathcal{V}_S$; otherwise (if $b = 1$), sample a non-member node $v \sim \mathcal{V} \setminus \mathcal{V}_S$.*
- 5) *Construct the input node-tuple:*

$$z_v := (\mathbf{x}_v, y_v, \mathcal{N}^L(v), \{\mathbf{x}_u : u \in \mathcal{N}^L(v)\}).$$

- 6) *Output 1 if $\mathcal{A}(\mathbf{x}_v, z_v, \Phi_S, \mathcal{G}_{\text{Adv}}) = b$, and 0 otherwise.*

Given the trained model Φ_S , node level query, \mathbf{x}_v , and its corresponding node-level tuple z_v constructed from adversary knowledge of its neighbors from some graph \mathcal{G}_{Adv} (which might not be same as \mathcal{G}_S), the goal of the adversary \mathcal{A} is to determine whether \mathbf{x}_v was part of the training set used to train the model Φ_S .

One would identify two important distinctions to the classical membership inference (MI) attacks as proposed by [14] affecting how threat models should be formulated.

First, the learning algorithm Φ operates not only on individual input samples but also on the relationships between them, encoded as a graph \mathcal{G}_S . This graph is typically constructed from the sampled node set S , and its topology plays a crucial role in the model's learning process. A simple approach might be to sample nodes uniformly at random to define S , which

then induces a subgraph \mathcal{G}_S . However, such graphs may lack connectivity or meaningful structural patterns, limiting the generalization capabilities of GNNs that rely on neighborhood aggregation. More realistic would be to use structured sampling strategies like *snowball sampling* [31], which start from a seed set of nodes $\mathcal{V}^{(0)}$ and iteratively expand by sampling neighbors of the current set. This yields more representative graph structures for downstream learning.

Second, and more importantly, the adversary’s capabilities must be clearly defined. In graph-based models, the prediction for a node depends not only on its own features but also on the features of its neighborhood. Thus, to meaningfully query the model Φ_S , an adversary must supply both the node features and a suitable neighborhood structure. The validity of any threat model hinges on assumptions about the adversary’s access to this neighborhood.

A concrete example is provided in [12], where a GNN is trained on a subset of a public social network to generate node representations. In such a scenario, the adversary has access to the full social network and attempts to infer which nodes were used during training. In other extreme case, an adversary may have only access to the node features without any knowledge of the neighborhood structure of a node.

Transductive vs. inductive settings : A further distinction concerns whether *test nodes are present during training*. In the **transductive** setting, the entire graph \mathcal{G} (nodes and edges) is available at training time, but labels are known only for the train nodes. The loss is computed on the labeled subset, yet the model can still aggregate information from *all* nodes—including those later treated as “test” nodes—through message passing. Consequently, the boundary between train and test is blurred: test nodes influence the learned representations via unlabeled (unsupervised) signals.

By contrast, in the **inductive** setting used in our study, train and test node sets are disjoint, and neither test nodes nor any train–test edges are exposed during training. We will see in Section VII how the choice of these settings combined with graph sampling strategy for sampling train nodes affect the statistical exchangeability of train/test nodes.

A. Attack Model

Existing works [4], [12], [32] typically employ a shadow model based [13] strategy to build the attack model. In particular, a shadow model is trained to mimic the target model. The shadow model employs a shadow dataset usually assumed to be sampled from the same distribution as the training dataset of the target model. The attack model is designed as a binary classification model, which maps the output posteriors of the shadow model on the shadow dataset $\mathcal{D}_{\text{shadow}}$ to the membership of the corresponding input member and non-member nodes.

To isolate the impact of the shadow dataset quality and different shadow model training methods from the influence of graph structure on the performance of membership inference (MI), we entirely skip the step of building the shadow model.

Instead, we give the adversary a significant advantage by providing the membership status of 80% of both the true member and non-member instances to the attackers. We only ask the attack model to predict the membership of the remaining samples.

For inferring membership of graph nodes we employ a 2-layer multilayer perceptron with ReLU activation as our attack model. The input to the attack model is the output posterior corresponding to the query node concatenated with the cross entropy loss value computed over the query node. Formally, let $\mathbf{p}(v)$ represent the output posterior for the query node v , and let $\mathcal{L}(v)$ denote the cross-entropy loss computed over v . The input to the attack model corresponding to node v is the concatenation of these two values, which can be written as:

$$\mathbf{x}_{\text{attack}} = [\mathbf{p}(v) \mid \mathcal{L}(v)].$$

Remark. Our goal is *not* to propose a new attack but to quantify how *edge structure* (employed during training–graph construction and inference-time edge access) affects membership advantage. The absolute success rate of any attack may change with attacker strength, model choices or defences (e.g., DP, calibration). Our focus, however, is on the *modulation* induced by edge structure. For this purpose, our setup using true membership for a large amount of data suffices to reveal the direction and relative magnitude of these edge-driven effects.

B. Evaluation using Membership Advantage

Following [14] we define the membership advantage of the attacker as the difference between the true and false positive rates of the \mathcal{A} :

$$\text{Adv}(\mathcal{A}) = \Pr(\mathcal{A} = 0 \mid b = 0) - \Pr(\mathcal{A} = 0 \mid b = 1)$$

We implement \mathcal{A} as a binary classifier which returns the probability of the input data point to be a member. We empirically compute the above advantage by taking the maximum of difference between the true and false positive rates of the classifier across all thresholds.

IV. DATASETS AND GRAPH SAMPLING STRATEGIES

A. Datasets

We perform our investigations on three popular graph datasets, namely CORA [33], CHAMELEON [34] and PUBMED [33] datasets. CORA and PUBMED are citation datasets where each research article is a node, and there exists an edge between two articles if one article cites the other. Each node has a label that shows the article category. In CORA, the features of each node are represented by a 0/1-valued word vector, which indicates the word’s presence or absence from the article’s abstract. In PUBMED, the node features are represented by the TF/IDF weighted word vector of the unique words in the dictionary.

CHAMELEON is a wikipedia network dataset. Nodes represent articles from the English Wikipedia, edges reflect mutual links between them. Node features indicate the presence of

TABLE I: Dataset statistics. $|\mathcal{V}|$ and $|\mathcal{E}|$ denote the number of nodes and (undirected) edges respectively, \mathcal{C} , d is the dimension of the feature vector.

	$ \mathcal{V} $	$ \mathcal{E} $	$ \mathcal{C} $	d	HOMOPHILY
CORA	2,708	5278	7	1,433	0.8252
CHAMELEON	2,277	31,371	5	2,325	0.2471
PUBMED	19,717	44,324	3	500	0.7924

particular nouns in the articles. The nodes were classified into 5 classes in terms of their average monthly traffic. All datasets are employed for the task of multi-class node classification.

The statistics of the datasets are provided in Table I. Here, we compute Average label homophily measures how often adjacent nodes share the same label.

For each node v with degree at least 1 we compute its label homophily as the fraction of its 1-hop neighbors which has the same label as v . We then compute average label homophily of the dataset (presented under HOMOPHILY in Table I) as the average label homophily of all non-isolated nodes. High homophily corresponds to connected nodes having the same labels whereas in heterophilic datasets such as CHAMELEON, connected nodes tend to have dissimilar labels.

B. Graph Sampling strategies

We employ two graph sampling strategies: *random sampling* and *snowball sampling*. These strategies determine not only which nodes are included in the training set but also the resulting graph topology, which in turn influences both model learning and the adversary’s ability to infer membership.

Random Sampling. Formally, given a graph $\mathcal{G} = (\mathcal{V}, \mathcal{E})$, where \mathcal{V} is the set of n nodes and \mathcal{E} is the set of m edges, we randomly sample N nodes independently and uniformly to form the sampled node set \mathcal{V}_S . The training graph is then constructed by including an edge (u, v) if and only if both $u, v \in \mathcal{V}_S$ and $(u, v) \in \mathcal{E}$.

Snowball Sampling. Here we start from an initial set of nodes $\mathcal{V}^{(0)}$ (in our experiments we randomly chose 10 nodes from each class to form $\mathcal{V}^{(0)}$). At each stage i we choose k neighbors of each of the nodes in $\mathcal{V}^{(i-1)}$. This is equivalent to obtaining a sample of incident edges of $\mathcal{V}^{(i-1)}$ which we denote by $\mathcal{E}^{(i)}$. We construct \mathcal{V}^i by adding only the new nodes discovered in the last stage. The process continues until the maximum number of nodes are sampled. The sampled train graph then is $\mathcal{G}_S = (\mathcal{V}_S, \mathcal{E}_S)$ where $\mathcal{V}_S = \cup_i \mathcal{V}^{(i)}$ and $\mathcal{E}_S = \cup_i \mathcal{E}^{(i)}$.

1) *Settings for generating training splits with snowball and random sampling.*: We sampled 5 train graphs each using snowball sampling and random sampling. For all datasets for all splits we fix the number of nodes in the train set to be 10% and 50% of the total nodes. In addition to the usual 50% split size adopted in evaluations in existing works we chose to include the 10% split size to simulate the real world setting of member data points (training nodes) usually much less than the overall population. For snowball sampling we build the initial node set $\mathcal{V}^{(0)}$ by selecting 10 nodes from each class

randomly. We fix $k = 3$ (number of maximum neighbors to be sampled from each selected node) for all datasets.

In Table II we provide mean of node degree over the train splits and the corresponding standard deviation as well as the average degree of the full graph. The average degrees corresponding to the full graphs are also provided.

TABLE II: Average degree of *train graphs* when 10% or 50% of nodes are sampled using SNOWBALL ($k=3$) or RANDOM and the underlying full graph without any sampling. Values are mean \pm std over 5 splits.

	Sampling Type	CORA	CHAMELEON	PUBMED
10%	SNOWBALL	1.68 ± 0.046	1.93 ± 0.052	2.55 ± 0.058
	RANDOM	0.34 ± 0.048	2.79 ± 0.495	0.41 ± 0.034
50%	SNOWBALL	3.18 ± 0.051	4.91 ± 0.143	3.55 ± 0.013
	RANDOM	2.00 ± 0.111	13.52 ± 0.741	2.21 ± 0.029
	FULL GRAPH	3.90 ± 0.00	27.55 ± 0.00	4.496 ± 0.00

V. INFLUENCE OF SAMPLING STRATEGY AND EDGE ACCESS

Before quantifying their effect on membership advantage (Sec. VI), we *motivate and justify our design choice* to vary two graph-specific factors *training-graph sampling* and *inference-time edge access* by systematically characterizing their impact on (i) the properties of sampled nodes, (ii) the distribution of model outputs, and (iii) the similarity (alignment) of predictive posteriors across adjacent nodes.

A. Characteristics of sampled nodes

From Table II we observe that snowball sampling leads to higher connectivity, except in the case of chameleon, where random samples are also well connected. In general, as we argue below snowball sampling biases the sample toward high-degree nodes, which affects both how representative the sample is and how GNN models behave.

With uniform random sampling, as studied in the current work, each node in the original graph is included in the sample independently with equal probability p . This implies that high-degree and low-degree nodes are sampled with equal likelihood. However, in the induced subgraph formed by the sampled nodes, high-degree nodes tend to appear with lower observed degrees. Specifically, a node of degree ℓ in the original graph will retain only those edges that connect to other sampled nodes. The probability that exactly k of its ℓ neighbors are also sampled follows a binomial distribution with parameters ℓ and p . Let P_ℓ denote the probability that a node has degree ℓ in the original graph, and let q_k denote the probability that a node has degree k in the sampled graph. Then, the degree distribution in the sampled graph is given by:

$$q_k = \sum_{\ell=k}^{\infty} \binom{\ell}{k} p^k (1-p)^{\ell-k} P_\ell, \quad (8)$$

This expression accounts for all nodes of degree $\ell \geq k$ in the original graph and computes the probability that exactly k of their neighbors are also sampled. As p decreases, the probability of retaining a high fraction of neighbors drops, leading to a shift in the degree distribution toward lower values.

In contrast, snowball sampling where sampling proceeds by recursively including neighbors of already sampled nodes tends to favor high-degree nodes. This is because such nodes have more opportunities to be reached during the expansion process, and once included, are more likely to bring in additional neighbors. To mitigate the bias toward high-degree nodes inherent in snowball sampling, we limit the number of neighbors sampled per node. This constraint helps control the average degree of the resulting subgraph, keeping it close to a predefined threshold and ensuring more balanced coverage. Nevertheless, the **probability of selecting a node in the training set increases with its degree** in case of snowball sampling whereas it stays uniform for the case of random sampling. From our above discussion we conclude that the way we construct the training graph does not just change which nodes are sampled (which is not critical as we can assume that their features are identically distributed), but more importantly their structural characteristics which introduces a distribution shift. This supports our argument that graph construction should be treated as an important factor when estimating privacy risks.

B. Node neighborhoods and output distributions

In addition to the influence of the edge structure during training, the output distributions of a GNN for the same set of query nodes can vary at inference time, even when the model parameters are fixed. This variation arises from the inherent *message-passing* or *aggregation* operation in GNNs (cf. Eq. (1)), which aggregates features from the node’s L -hop neighborhood. We consider three types of graph access at inference time:

- **ORIG:** Only the original train edges and test edges are used; train and test sets are edge-disjoint.
- **ALLEDGES:** All edges from the underlying graph—including edges between train and test nodes—are used during inference.
- **NOGRAPH:** The graph structure is not used at all during inference.

Let Φ be a fixed trained GNN model, and let v be a query node. Let $\mathcal{N}_{G_1}^L(v)$ and $\mathcal{N}_{G_2}^L(v)$ denote the L -hop neighborhoods of node v in two graphs G_1 and G_2 that differ in edge structure (e.g., different sampling strategies or inference-time neighborhood truncation). Then, the model’s output for v under these two neighborhoods is given by:

$$\mathbf{y}_v^{(1)} := \Phi(v; \mathcal{N}_{G_1}^L(v)) \quad \text{and} \quad \mathbf{y}_v^{(2)} := \Phi(v; \mathcal{N}_{G_2}^L(v)).$$

We compute the KL-divergence between the two posteriors to capture the discrepancy in the model’s output for the same node under different neighborhood contexts:

$$\mathcal{D}(v; G_1, G_2) := D_{KL}(\mathbf{y}_v^{(1)} || \mathbf{y}_v^{(2)}).$$

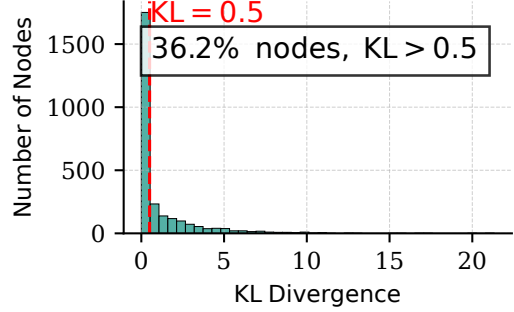


Fig. 1: Distribution of KL divergence among posterior distribution of nodes on CORA dataset comparing the cases when all edges and none of the edges were used during inference. The model (GCN) was trained on a **snowball** sampled split with 50% of the nodes in the train set.

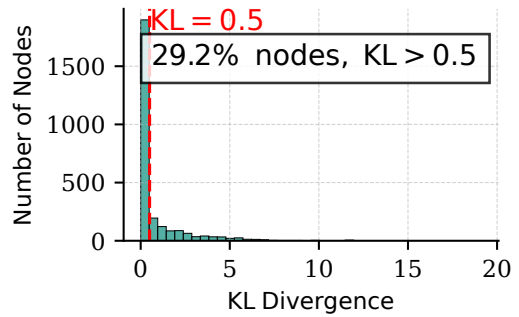


Fig. 2: Distribution of KL divergence among posterior distribution of nodes on CORA dataset comparing the cases when all edges and none of the edges were used during inference. The model (GCN) was trained on a **randomly** sampled split with 50% of the nodes in the train set.

This divergence can be non-zero even for nodes in the training set, highlighting that inference-time neighborhood construction has a direct and potentially significant impact on model predictions. An extreme illustration of this occurs when all neighbors are included during inference versus when all edges are ignored resulting in entirely different aggregation contexts and hence different predictions. In Figures 1 and 2, we show how the output posterior distribution changes for the same nodes and model when only the neighborhood structure is varied.

C. Impact on posterior similarity of adjacent nodes

Because message passing mixes neighboring node features, many GNNs produce similar posterior distributions for adjacent nodes in the inference graph. The extent of this “posterior smoothing” depends on the aggregation mechanism (e.g., mean, max, LSTM) and model architecture. To quantify it, we compute the Jensen–Shannon (JS) divergence between each node’s posterior and the posteriors of its neighbors (using edges assigned to the train and test splits), and average over

neighbors to obtain a per-node score. Lower JS indicates stronger similarity. This matters for membership inference: if an attack model uses posteriors as features, lower JS makes neighboring nodes more likely to receive the same membership label (member or non-member), so correctly identifying one node can carry over to its neighbors. In Figure 3 we plot the empirical cumulative distribution function for JS-divergence of posteriors of adjacent nodes (according to the original split ORIG) when at inference different settings of edge access are applied. As expected, ECDF is lowest when no edges are used at inference, except for GRAPHsAGE, where neighboring nodes remain less distinguishable even without edges.

D. Distribution of true class confidence

For each node, we map the posterior confidence $p \in (0, 1)$ to the *log-odds* (logit)

$$z = \text{logit}(p) = \log\left(\frac{p}{1-p}\right).$$

This places probabilities on an unbounded, symmetric scale ($z = 0$ at $p = 0.5$; $z > 0$ iff $p > 0.5$), which spreads out extreme values near 0/1 and facilitates distributional comparisons [19]. To avoid infinities at $p \in \{0, 1\}$, we clamp $p \leftarrow \min(\max(p, \varepsilon), 1 - \varepsilon)$ with $\varepsilon = 10^{-6}$ before applying the transform. (The inverse mapping is the sigmoid $p = \sigma(z) = 1/(1 + e^{-z})$.) As Figure 3 shows, even when no edges are used at inference, GRAPHsAGE posteriors can still separate member from non-member nodes (though not necessarily into the correct classes). This raises the question: do class confidence scores (used as a proxy for loss) also retain this distinguishability? In Figure 4 we plot the distribution for logit transformed true class confidence scores for the same dataset as in the previous section with GRAPHsAGE under different edge access settings. The scores provide greater distinguishability when edges from the original split (as opposed to what we observed for posterior distributions) are included at inference compared to the other settings.

VI. GRAPH STRUCTURE AND MEMBERSHIP ADVANTAGE

We now present large-scale experiments on how edge structure impacts membership advantage in GNNs. We begin by analyzing the effect of our two design choices, *training-graph construction* and *inference-time edge access*, on predictive performance (Section VI-B), and then study how the resulting train–test performance gap correlates with membership advantage.

A. Experimental setup

For each dataset we perform our experiments on 5 training splits constructed using snowball sampling and random sampling as described in Section IV. The attack model is a 2-layer MLP trained on 80% of member and non-member data points with their true labels. For each of the training-test data split of the target model, we generate 3 random splits for the attack model with 80% labelled data. The attack results are then summarized over a total of 15 runs for each dataset.

We employ performance gap between the train and test sets to approximate generalization gap. We compute the performance gap as the percentage decrease in test accuracy relative to the training accuracy, i.e.,

$$\Delta_{\text{gen}} = \frac{ACC_{\text{train}} - ACC_{\text{test}}}{ACC_{\text{train}}} \times 100.$$

We consider three types of graph access at inference time:

- **ORIG**: Only the original train edges and test edges are used; train and test sets are edge-disjoint.
- **ALLEDGES**: All edges from the underlying graph—including edges between train and test nodes—are used during inference.
- **NOGRAPH**: The graph structure is not used at all during inference.

Even when the set of member (train) and non-member (test) nodes is fixed, the level of access to the graph structure during inference can significantly affect observed train and test performance.

B. How do graph sampling and edge access affect performance gap?

Figures 5a, 6a and 7a present the results on performance gap of the three GNNs under two train-graph construction strategies and the different edge access levels. Detailed scores corresponding to the presented figures are provided in the Appendix.

1) *Effect of sampling type*: When comparing different sampling strategies for constructing the training graph, we would expect higher performance gap when train graphs are snowball sampled. The rationale behind this is that with random sampling, despite disrupting the graph structure, we obtain a i.i.d. node distribution. In contrast, snowball sampling introduces bias by expanding from a seed set, increasing the likelihood of sampling nodes that are structurally similar or closely connected. While the expected trend is observed over all datasets there are a few exceptions for smaller train sizes.

2) *Effect of edge access*: The performance gap varies depending on the level of graph access. The gap is usually smallest when all edges are used (ALLEDGES) and largest when no edges are used (NOGRAPH). This highlights the benefit of including inter-train-test edges in improving test-time predictions. There are again a few exceptions mainly for PUBMED when performance gap using the original split is higher than using no edges which might indicate that features alone might be more informative for the task at hand.

3) *Effect of sampling size*: When the number of training nodes is increased from 10% to 50% decrease in performance gap as expected is observed (with minor exceptions) for all models at different graph access levels and train sampling strategies.

C. How does performance gap translate to membership advantage?

Figures 5b–7b summarize membership advantage scores across all evaluated attacks and datasets, following the setup in

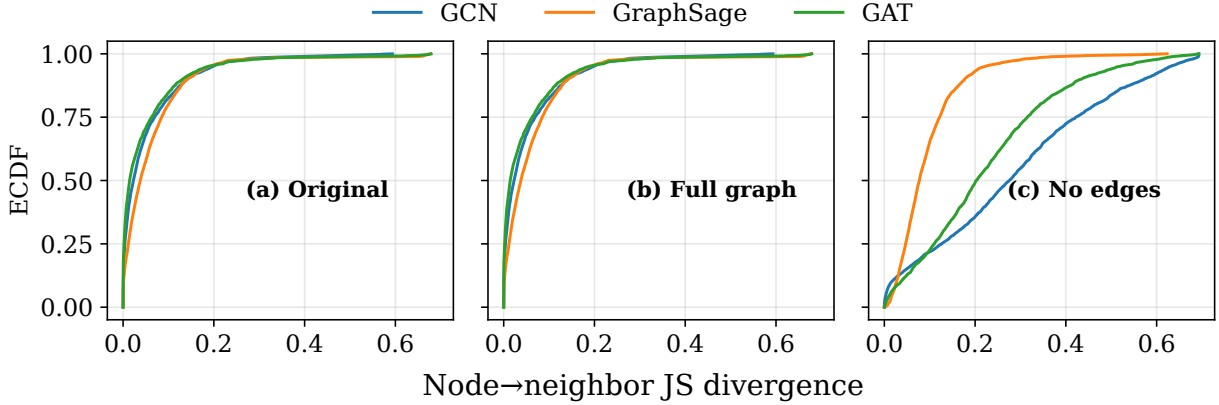


Fig. 3: Empirical cumulative distribution function of JS divergence for the three models under different access level settings. Dataset used here is CORA with 10% nodes in train split sampled using snowball sampling. The JS divergence is computed between the query’s and neighbors posterior distribution where two nodes are considered when an edge is present between them according to the original split, i.e., no edges are present between the train and test nodes. Overall, one would expect ECDF to be lowest when none of the edges are used during inference. GRAPHsAGE shows an exception where posterior distribution of neighboring nodes are less distinguishable even when none of the edges are included in the inference stage.

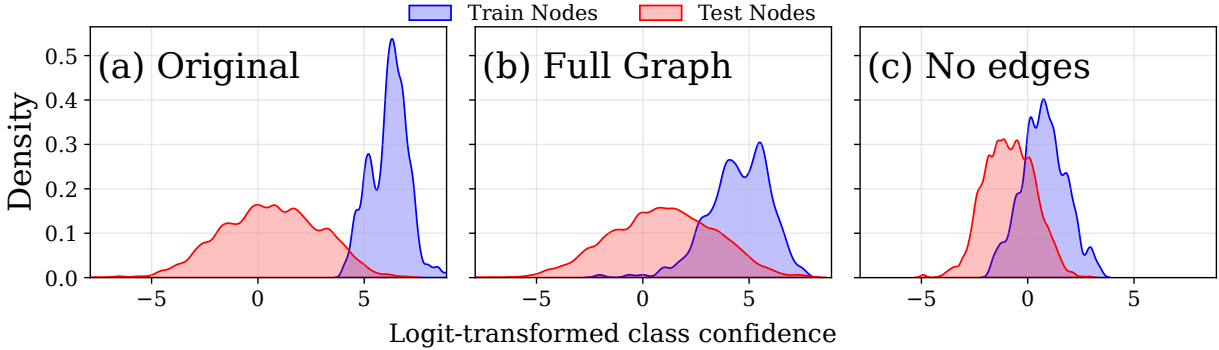


Fig. 4: Effect of edge structure on train–test separability of class confidence (log-odds of the true-class posterior) for a GRAPHsAGE model. The model was trained over CORA dataset with 10% of nodes sampled for training using **snowball** sampling. We compare three inference graphs: (a) *Original* (train/test edge sets disjoint), (b) *Full graph* (all edges available), and (c) *No edges*. Train (blue) and test (red) distributions are most separated in (a), indicating stronger distinguishability; in (b) and (c) they overlap more, indicating weaker distinguishability.

Section VI-A. When the overall trend holds that membership advantage is positively correlated with high membership advantage there are more nuances introduced by different graph access levels. Specifically, if we observe highest performance gap when no edges are used, the membership advantage in this case still stays lower than in the case of using original split for CORA and CHAMELEON datasets. Moreover, the differences in membership advantage in CORA and CHAMELEON at different edge access level are lowest for GRAPHsAGE. We hypothesize this stems from GRAPHsAGE’s concatenation of the node’s own embedding with the aggregated neighborhood, preserving node-specific signal and making GRAPHsAGE less sensitive to biased neighbor sets than GCN/GAT, which directly mix node and neighbor messages.

Even more interesting case is that of PUBMED. Though

overall performance gap and membership advantage for different models is the lowest for PUBMED, we observe that for snowball sampled train graphs the membership advantage when using all edges for inference when using GCN is much higher than when using original split for inference. This effect cannot be explained by performance gap as performance gap is close to 0 when using all edges for this particular case.

Overall our experimental results point to the fact that the edge structure is a crucial variable for understanding and quantifying privacy leakage. Alone performance or generalization gap does not suffice to explain the information leakage in graph based models. For realistic evaluation of privacy leakage in GNNs we need to devise new and realistic assumptions on the available graph structure to the adversary. To develop more intelligent attacks new edge manipulation strategies

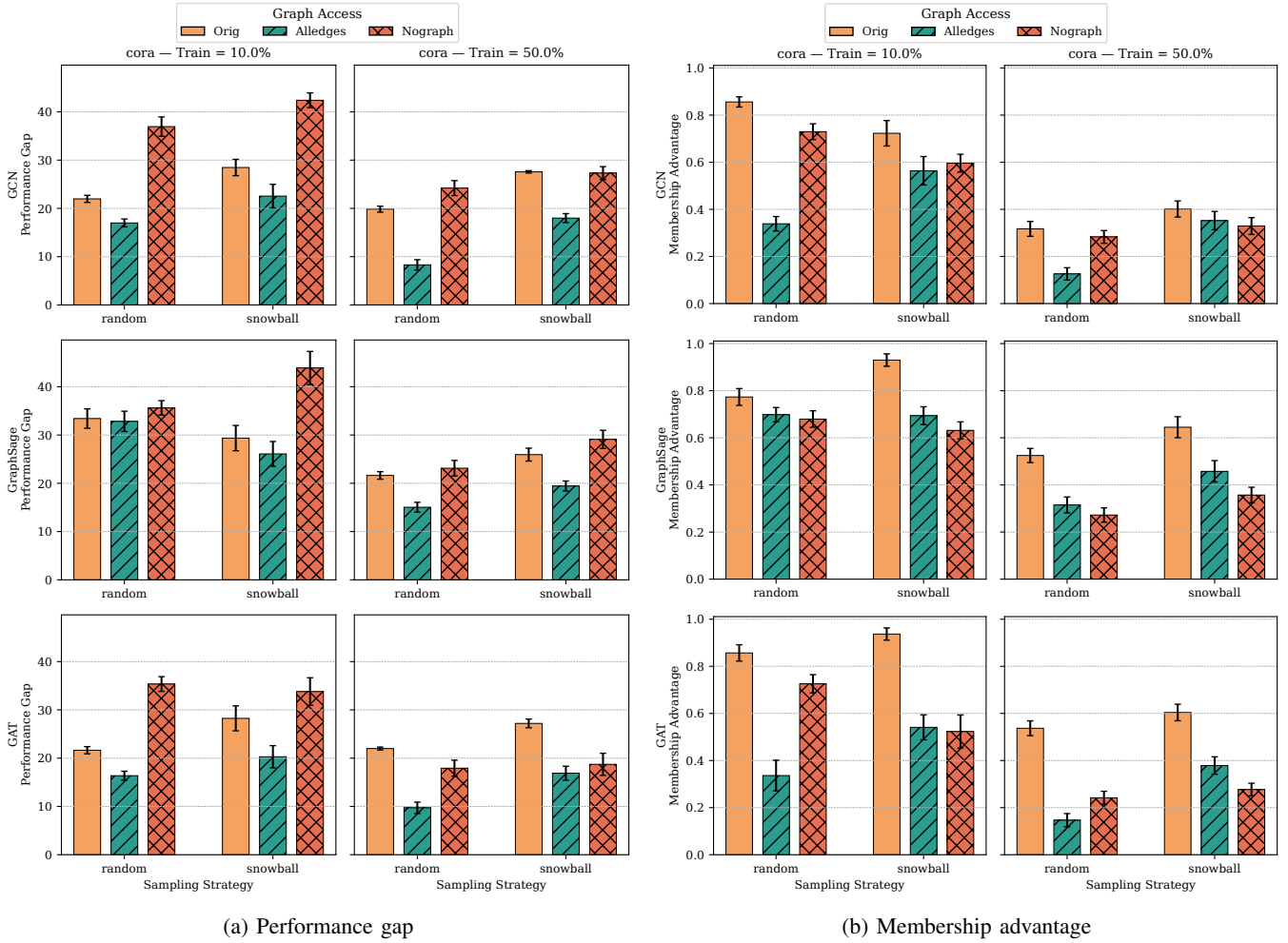


Fig. 5: (a) Performance gap and (b) membership advantage on the CORA dataset at different train sizes (10% (l) and 50% (r)).

would need to be developed that can help attacker to behave differently on member and non-member query nodes.

VII. IMPLICATIONS FOR BOUNDING MEMBERSHIP ADVANTAGE OF DIFFERENTIAL PRIVATE MODELS

We argue that, beyond the practical challenges of evaluating privacy attacks, the edge structure of graphs adds a significant and unavoidable complexity to privacy auditing. The membership advantage of $(\varepsilon, 0)$ -differentially private models [14] is bounded as $Adv \leq e^\varepsilon - 1$ for loss-based attacks. [15] further improves this bound and demonstrates that for such bounds to be applicable, the train and test samples must be statistically exchangeable.

In the following, we reproduce and adapt the definition of statistical exchangeability from [15] to the setting of message passing graph neural networks (GNNs) as described in Section II-A, where each data instance includes not only a node's features but also its local neighborhood structure.

Definition 2 (Statistical Exchangeability in MI for GNNs). *Let \mathcal{D} denote a joint distribution over n member samples*

$\{z_1, \dots, z_n\}$ and a non-member sample z_{n+1} , where each sample z_v corresponds to a tuple:

$$z_v := (\mathbf{x}_v, y_v, \mathcal{N}_{G'}^L(v), \{\mathbf{x}_u : u \in \mathcal{N}_{G'}^L(v)\}),$$

with \mathbf{x}_v being the feature vector of node x_v , y_v its label, and $\mathcal{N}_{G'}^L(v)$ denoting the L -hop neighborhood of v in a graph view G' . The graph G' may correspond to the full graph G , or to a subgraph induced by the sampled training node set with edges included according to a specific sampling scheme such as random or snowball sampling.

We say that \mathcal{D} is statistically exchangeable if the joint distribution over all samples $\{z_1, \dots, z_{n+1}\} \sim \mathcal{D}$ is invariant under permutations of sample indices. That is, for any permutation $\sigma : [n+1] \rightarrow [n+1]$, it holds that:

$$\Pr(z_1, \dots, z_{n+1}) = \Pr(z_{\sigma(1)}, \dots, z_{\sigma(n+1)}). \quad (9)$$

Theorem 1. *Let \mathcal{D} be a joint distribution over n member samples $\{z_1, \dots, z_n\}$ and a non-member sample z_{n+1} , where each sample z_v is defined as in Definition 2, and where neighborhoods $\mathcal{N}_{G'}^L(v)$ are computed over a graph view G' constructed via a node sampling scheme. Then \mathcal{D} is not always*

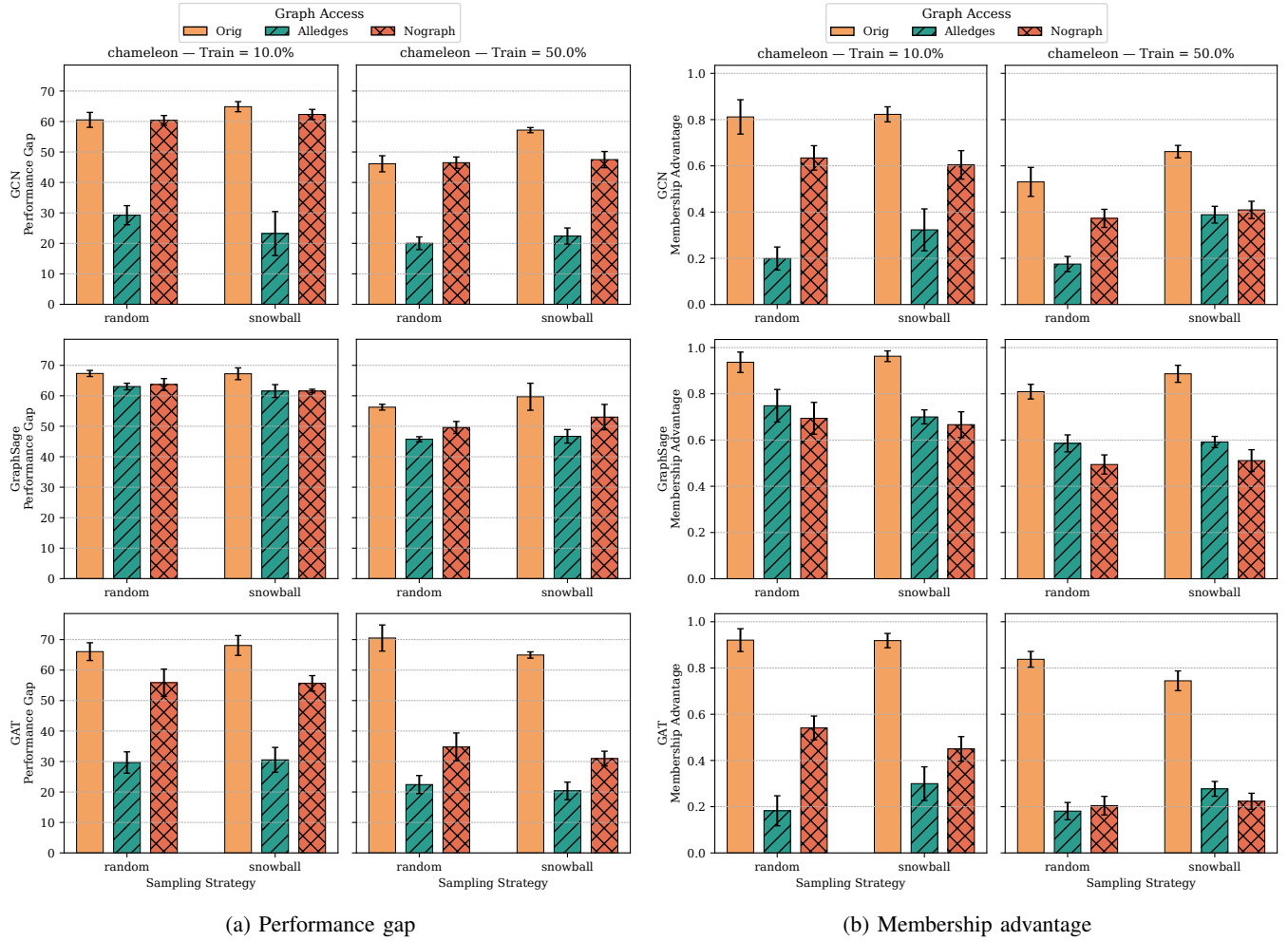


Fig. 6: Performance gap and Membership advantage for CHAMELEON dataset at different train set sizes (10% (l) and 50% (r)).

guaranteed to be statistically exchangeable if G' is a subgraph constructed over the a sampled set of training nodes $S \subset V$, and $\mathcal{N}_{G'}^L(v)$ is restricted to lie within S .

Proof. We consider two inductive sampling schemes as studied in this work: random node sampling and snowball sampling.

Case 1: Random Node Sampling. Let G' denote the subgraph induced over the training node set $S = \{x_1, \dots, x_n\}$, and let the joint sample sequence be $Z = (z_1, \dots, z_n, z_{n+1})$, where each z_v is defined as in Definition 2.

Now consider a permutation $Z^\sigma = (z_{\sigma(1)}, \dots, z_{\sigma(n+1)})$ in which the non-member node x_{n+1} replaces some member node $x_i \in S$. The resulting training set becomes:

$$S' = \{x_1, \dots, x_{i-1}, x_{n+1}, x_{i+1}, \dots, x_n\},$$

and we define the new induced subgraph as G'' . Since neighborhoods $\mathcal{N}_G^L(v)$ depend on the underlying graph, we have:

$$\mathcal{N}_{G'}^L(v) \neq \mathcal{N}_{G''}^L(v) \quad \text{for some } v \in S \cup \{x_{n+1}\},$$

unless both the exchanged nodes are isolated in the original graph G . Thus, the permuted tuple Z^σ becomes incompatible with the graph structure G'' , and so:

$$\Pr(Z^\sigma \mid G') = 0, \quad \text{while} \quad \Pr(Z \mid G') > 0.$$

Since the graph view G' is generated by the sampling process with non-zero probability, i.e., $\Pr(G') > 0$, it follows that the joint distribution is not invariant under permutation:

$$\Pr(Z) \neq \Pr(Z^\sigma),$$

violating statistical exchangeability.

Case 2: Snowball Sampling. Let G' be the subgraph generated using a snowball sampling process starting from a seed node set while sampling a fixed number of neighbors for each selected node in each iteration. In this setting, the set of sampled nodes and edges depends on the order in which nodes are traversed.

Now consider a permutation Z^σ where the non-member node x_{n+1} replaces a member node x_i . The resulting training set becomes:

$$S' = \{x_1, \dots, x_{i-1}, x_{n+1}, x_{i+1}, \dots, x_n\}.$$

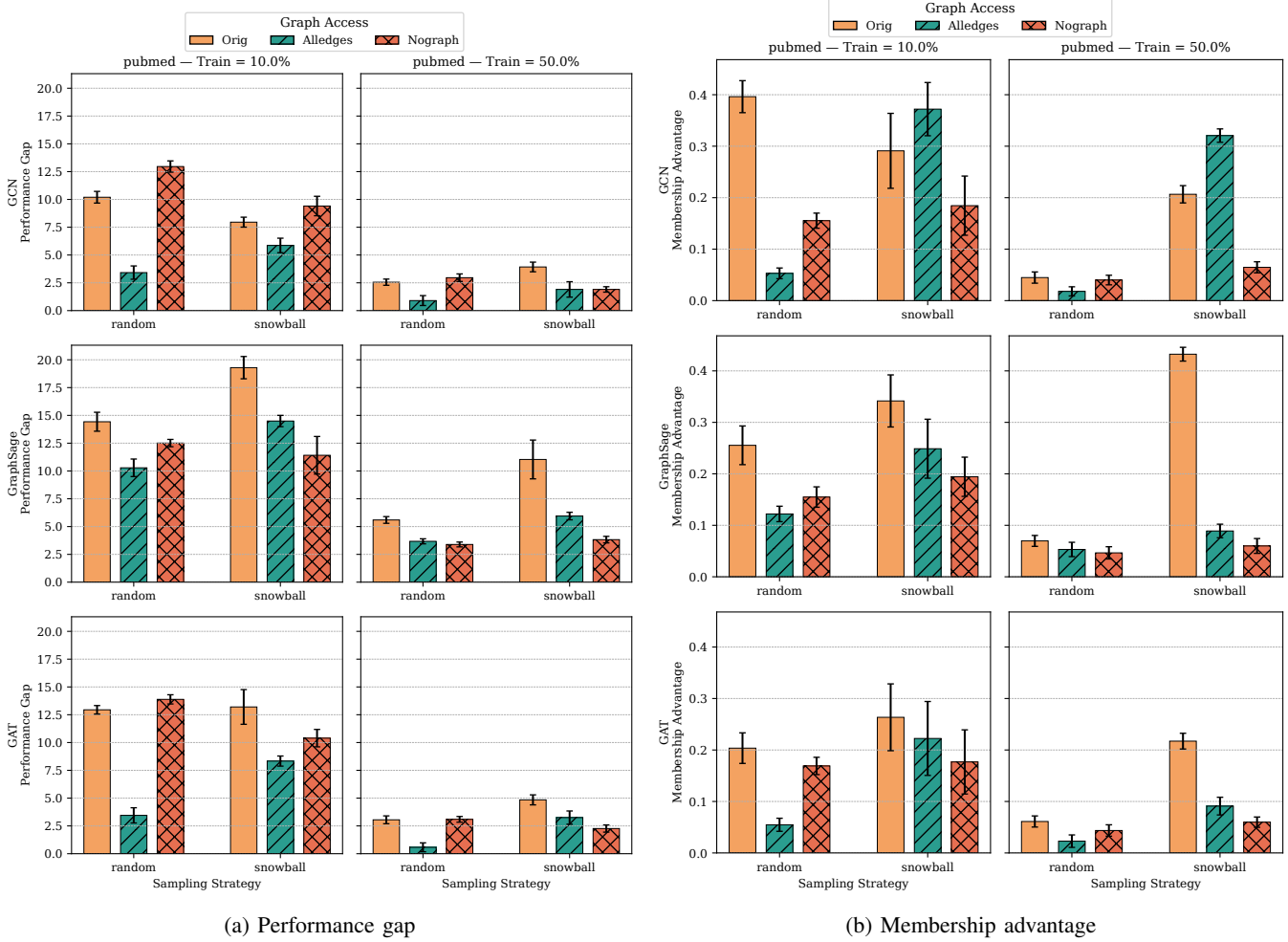


Fig. 7: Performance gap and Membership advantage for PUBMED dataset at different train set sizes (10% (l) and 50% (r)).

Snowball sampling proceeds in layers by expanding neighbors of already sampled nodes. This means that whether a node is even included in the final subgraph depends on the specific sequence in which other nodes were included before it. Therefore, replacing x_i with x_{n+1} can not only alter neighborhoods but may also cause some nodes that were previously sampled to no longer appear in G'' , and vice versa.

As a result, the neighborhood $\mathcal{N}_{G''}^L(v)$ and even the support of Z^σ may differ fundamentally (in terms of node features) from that of Z , and under a fixed G' , we have:

$$\Pr(Z^\sigma | G') = 0, \quad \text{while} \quad \Pr(Z | G') > 0.$$

Thus, snowball sampling also violates statistical exchangeability due to its sequential and history-dependent nature. \square

From the above discussion, we conclude that in inductive train-test splits, where the neighborhood structure of the training graph is determined by the set of sampled training nodes, statistical exchangeability between training and test samples cannot be always guaranteed. In contrast, in transductive settings, where the full graph G is accessible and fixed during training thus decoupling neighborhood structure from

the sampled training nodes, statistical exchangeability holds when the training nodes are sampled randomly.

However, if snowball sampling is used to select training nodes, even when the full graph G is utilized during training, statistical exchangeability is still violated. This is because node inclusion under snowball sampling depends on the initial seed set and the traversal order, making the set of training nodes itself order-dependent.

VIII. CONCLUSION

We investigated node-level membership inference (MI) against GNNs in the inductive setting, formalizing the problem via a joint distribution over node–neighborhood tuples and an explicit membership inference experiment. Our large-scale evaluation across datasets, training-graph construction strategies, edge-access regimes, and model families shows that inference-time edge access and the training-graph construction strategy are dominant determinants of privacy risk. Although the generalization gap correlates with membership advantage, it is an insufficient proxy where edge access level and sampling bias can dominate. Finally, while more graph-specific attacks

are needed to assess realistic risks, the statistical interdependence induced by edges undermines the common practice of inferring lower bounds on information leakage in differentially private models from attack success rates alone, calling for graph-aware privacy auditing protocols.

REFERENCES

- [1] T. Gaudeflot, B. Day, A. R. Jamasb, J. Soman, C. Regep, G. Liu, J. B. Hayter, R. Vickers, C. Roberts, J. Tang *et al.*, “Utilizing graph machine learning within drug discovery and development,” *Briefings in bioinformatics*, vol. 22, no. 6, p. bbab159, 2021.
- [2] R. Schulte-Sasse, S. Budach, D. Hnisz, and A. Marsico, “Integration of multiomics data with graph convolutional networks to identify new cancer genes and their associated molecular mechanisms,” *Nature Machine Intelligence*, vol. 3, no. 6, pp. 513–526, 2021.
- [3] A. Sanchez-Gonzalez, J. Godwin, T. Pfaff, R. Ying, J. Leskovec, and P. Battaglia, “Learning to simulate complex physics with graph networks,” in *International Conference on Machine Learning*. PMLR, 2020, pp. 8459–8468.
- [4] V. Duddu, A. Boutet, and V. Shejwalkar, “Quantifying privacy leakage in graph embedding,” in *MobiQuitous 2020-17th EAI International Conference on Mobile and Ubiquitous Systems: Computing, Networking and Services*, 2020, pp. 76–85.
- [5] M. Conti, J. Li, S. Picek, and J. Xu, “Label-only membership inference attack against node-level graph neural networks,” in *Proceedings of the 15th ACM Workshop on Artificial Intelligence and Security*, 2022, pp. 1–12.
- [6] X. He, J. Jia, M. Backes, N. Z. Gong, and Y. Zhang, “Stealing links from graph neural networks,” in *30th USENIX security symposium (USENIX security 21)*, 2021, pp. 2669–2686.
- [7] A. Jnaini, A. Bettar, and M. A. Koulali, “How powerful are membership inference attacks on graph neural networks?” in *Proceedings of the 34th International Conference on Scientific and Statistical Database Management*, 2022, pp. 1–4.
- [8] X. Wang and W. H. Wang, “Subgraph structure membership inference attacks against graph neural networks,” *Proceedings on Privacy Enhancing Technologies*, 2024.
- [9] B. Wu, X. Yang, S. Pan, and X. Yuan, “Adapting membership inference attacks to gnn for graph classification: Approaches and implications,” in *2021 IEEE International Conference on Data Mining (ICDM)*. IEEE, 2021, pp. 1421–1426.
- [10] E. Dai, T. Zhao, H. Zhu, J. Xu, Z. Guo, H. Liu, J. Tang, and S. Wang, “A comprehensive survey on trustworthy graph neural networks: Privacy, robustness, fairness, and explainability,” *arXiv preprint arXiv:2204.08570*, 2022.
- [11] Y. Wang, L. Huang, P. S. Yu, and L. Sun, “Membership inference attacks on knowledge graphs,” *arXiv preprint arXiv:2104.08273*, 2021.
- [12] I. E. Olatunji, W. Nejdl, and M. Khosla, “Membership inference attack on graph neural networks,” in *2021 Third IEEE International Conference on Trust, Privacy and Security in Intelligent Systems and Applications (TPS-ISA)*. IEEE, 2021, pp. 11–20.
- [13] R. Shokri, M. Stronati, C. Song, and V. Shmatikov, “Membership inference attacks against machine learning models,” in *2017 IEEE symposium on security and privacy (SP)*. IEEE, 2017, pp. 3–18.
- [14] S. Yeom, I. Giacomelli, M. Fredrikson, and S. Jha, “Privacy risk in machine learning: Analyzing the connection to overfitting,” in *2018 IEEE 31st computer security foundations symposium (CSF)*. IEEE, 2018, pp. 268–282.
- [15] T. Humphries, S. Oya, L. Tulloch, M. Rafuse, I. Goldberg, U. Hengartner, and F. Kerschbaum, “Investigating membership inference attacks under data dependencies,” in *2023 IEEE 36th Computer Security Foundations Symposium (CSF)*. IEEE, 2023, pp. 473–488.
- [16] T. N. Kipf and M. Welling, “Semi-supervised classification with graph convolutional networks,” in *5th International Conference on Learning Representations, ICLR 2017*, 2017.
- [17] W. Hamilton, Z. Ying, and J. Leskovec, “Inductive representation learning on large graphs,” *Advances in neural information processing systems*, vol. 30, 2017.
- [18] P. Veličković, G. Cucurull, A. Casanova, A. Romero, P. Lio, and Y. Bengio, “Graph attention networks,” *arXiv preprint arXiv:1710.10903*, 2017.
- [19] N. Carlini, S. Chien, M. Nasr, S. Song, A. Terzis, and F. Tramer, “Membership inference attacks from first principles,” in *2022 IEEE Symposium on Security and Privacy (SP)*. IEEE, 2022, pp. 1897–1914.
- [20] A. Salem, Y. Zhang, M. Humbert, P. Berrang, M. Fritz, and M. Backes, “MI-leaks: Model and data independent membership inference attacks and defenses on machine learning models,” *arXiv preprint arXiv:1806.01246*, 2018.
- [21] H. Hu, Z. Salcic, L. Sun, G. Dobbie, P. S. Yu, and X. Zhang, “Membership inference attacks on machine learning: A survey,” *ACM Computing Surveys (CSUR)*, vol. 54, no. 11s, pp. 1–37, 2022.
- [22] C. Dwork, F. McSherry, K. Nissim, and A. Smith, “Calibrating noise to sensitivity in private data analysis,” in *Theory of cryptography conference*. Springer, 2006, pp. 265–284.
- [23] N. Papernot, S. Song, I. Mironov, A. Raghunathan, K. Talwar, and U. Erlingsson, “Scalable private learning with pate,” *arXiv preprint arXiv:1802.08908*, 2018.
- [24] I. E. Olatunji, T. Funke, and M. Khosla, “Releasing graph neural networks with differential privacy guarantees,” *Transactions on Machine Learning Research*, 2023.
- [25] M. Abadi, A. Chu, I. Goodfellow, H. B. McMahan, I. Mironov, K. Talwar, and L. Zhang, “Deep learning with differential privacy,” in *Proceedings of the 2016 ACM SIGSAC Conference on Computer and Communications Security*, ser. CCS ’16. New York, NY, USA: Association for Computing Machinery, 2016, p. 308–318. [Online]. Available: <https://doi.org/10.1145/2976749.2978318>
- [26] Z. Xiang, T. Wang, and D. Wang, “Preserving node-level privacy in graph neural networks,” in *2024 IEEE Symposium on Security and Privacy (SP)*. IEEE, 2024, pp. 4714–4732.
- [27] S. Sajadmanesh, A. S. Shamsabadi, A. Bellet, and D. Gatica-Perez, “Gap: Differentially private graph neural networks with aggregation perturbation,” *arXiv preprint arXiv:2203.00949*, 2022.
- [28] S. Sajadmanesh and D. Gatica-Perez, “Locally private graph neural networks,” in *Proceedings of the 2021 ACM SIGSAC Conference on Computer and Communications Security*, 2021, pp. 2130–2145.
- [29] B. Jayaraman and D. Evans, “Evaluating differentially private machine learning in practice,” in *28th USENIX security symposium (USENIX security 19)*, 2019, pp. 1895–1912.
- [30] M. Jagielski, J. Ullman, and A. Oprea, “Auditing differentially private machine learning: How private is private sgd?” *Advances in Neural Information Processing Systems*, vol. 33, pp. 22 205–22 216, 2020.
- [31] J. Leskovec and C. Faloutsos, “Sampling from large graphs,” in *Proceedings of the 12th ACM SIGKDD international conference on Knowledge discovery and data mining*, 2006, pp. 631–636.
- [32] X. He, R. Wen, Y. Wu, M. Backes, Y. Shen, and Y. Zhang, “Node-level membership inference attacks against graph neural networks,” *arXiv preprint arXiv:2102.05429*, 2021.
- [33] P. Sen, G. Namata, M. Bilgic, L. Getoor, B. Galligher, and T. Eliassi-Rad, “Collective classification in network data,” *AI magazine*, vol. 29, no. 3, pp. 93–93, 2008.
- [34] B. Rozemberczki, C. Allen, and R. Sarkar, “Multi-scale attributed node embedding,” 2019.

APPENDIX

In the following we present detailed performance scores, performance gaps and membership advantage for different models and datasets under different settings.

TABLE III: Performance on CORA with 10% nodes in the train set sampled using (a) random sampling and (b) snowball sampling.

Model	Metric	Random			Snowball		
		ORIGINAL SPLIT	FULL GRAPH	NO EDGES	ORIGINAL SPLIT	FULL GRAPH	NO EDGES
GCN	TRAIN ACC	0.9889 \pm 0.0057	0.9541 \pm 0.0123	0.9926 \pm 0.0052	0.9970 \pm 0.0043	0.9644 \pm 0.0130	0.9504 \pm 0.0151
	TEST ACC	0.7716 \pm 0.0102	0.7920 \pm 0.0110	0.6259 \pm 0.0202	0.7151 \pm 0.0134	0.7472 \pm 0.0149	0.5480 \pm 0.0194
GRAPH SAGE	TRAIN ACC	1.0000 \pm 0.0000	1.0000 \pm 0.0000	0.9815 \pm 0.0070	1.0000 \pm 0.0000	1.0000 \pm 0.0000	0.9393 \pm 0.0093
	TEST ACC	0.6684 \pm 0.0202	0.6742 \pm 0.0217	0.6329 \pm 0.0172	0.7074 \pm 0.0266	0.7392 \pm 0.0252	0.5221 \pm 0.0455
GAT	TRAIN ACC	0.9874 \pm 0.0044	0.9385 \pm 0.0173	0.9793 \pm 0.0018	0.9941 \pm 0.0038	0.9230 \pm 0.0220	0.8822 \pm 0.0160
	TEST ACC	0.7716 \pm 0.0132	0.7894 \pm 0.0075	0.6327 \pm 0.0196	0.7171 \pm 0.0095	0.7445 \pm 0.0100	0.5736 \pm 0.0209

TABLE IV: Train and test accuracies on CORA with 50% nodes in the train set sampled using (a) random sampling (left) and (b) snowball sampling (right) . Values are mean \pm std.

Model	Metric	Random			Snowball		
		ORIGINAL SPLIT	FULL GRAPH	NO EDGES	ORIGINAL SPLIT	FULL GRAPH	NO EDGES
GCN	TRAIN ACC	0.9885 \pm 0.0018	0.9492 \pm 0.0072	0.8953 \pm 0.0058	0.9959 \pm 0.0017	0.9715 \pm 0.0041	0.8415 \pm 0.0068
	TEST ACC	0.7923 \pm 0.0060	0.8703 \pm 0.0076	0.6786 \pm 0.0156	0.7220 \pm 0.0027	0.7973 \pm 0.0074	0.6130 \pm 0.0172
GRAPH SAGE	TRAIN ACC	1.0000 \pm 0.0000	0.9931 \pm 0.0022	0.8922 \pm 0.0141	1.0000 \pm 0.0000	0.9975 \pm 0.0006	0.8959 \pm 0.0089
	TEST ACC	0.7838 \pm 0.0078	0.8437 \pm 0.0105	0.6857 \pm 0.0071	0.7405 \pm 0.0124	0.8062 \pm 0.0087	0.6346 \pm 0.0167
GAT	TRAIN ACC	0.9911 \pm 0.0026	0.9329 \pm 0.0093	0.8442 \pm 0.0064	0.9939 \pm 0.0043	0.9517 \pm 0.0052	0.7948 \pm 0.0098
	TEST ACC	0.7731 \pm 0.0037	0.8422 \pm 0.0094	0.6928 \pm 0.0097	0.7182 \pm 0.0090	0.7818 \pm 0.0102	0.6399 \pm 0.0125

TABLE V: Train and test accuracies on CHAMELEON with 10% nodes in the train set sampled using (a) random sampling (left) and (b) snowball sampling (right) . Values are mean \pm std.

Model	Metric	Random			Snowball		
		ORIGINAL SPLIT	FULL GRAPH	NO EDGES	ORIGINAL SPLIT	FULL GRAPH	NO EDGES
GCN	TRAIN ACC	0.9480 \pm 0.0135	0.5753 \pm 0.0154	0.8617 \pm 0.0210	0.9894 \pm 0.0082	0.5260 \pm 0.0540	0.8379 \pm 0.0401
	TEST ACC	0.3742 \pm 0.0259	0.4070 \pm 0.0201	0.3414 \pm 0.0126	0.3477 \pm 0.0179	0.4004 \pm 0.0214	0.3154 \pm 0.0149
GRAPH SAGE	TRAIN ACC	0.9921 \pm 0.0051	0.9339 \pm 0.0306	0.8511 \pm 0.0161	0.9956 \pm 0.0039	0.9410 \pm 0.0194	0.8696 \pm 0.0581
	TEST ACC	0.3240 \pm 0.0091	0.3449 \pm 0.0107	0.3091 \pm 0.0190	0.3262 \pm 0.0198	0.3619 \pm 0.0239	0.3340 \pm 0.0206
GAT	TRAIN ACC	0.9436 \pm 0.0156	0.5304 \pm 0.0296	0.7542 \pm 0.0242	0.9771 \pm 0.0213	0.4793 \pm 0.0304	0.6467 \pm 0.0360
	TEST ACC	0.3200 \pm 0.0263	0.3726 \pm 0.0204	0.3329 \pm 0.0358	0.3112 \pm 0.0261	0.3324 \pm 0.0218	0.2870 \pm 0.0249

TABLE VI: Train and test accuracies on CHAMELEON with 50% nodes in training set. Left block: random sampling; right block: snowball sampling. Values are mean \pm std.

Model	Metric	Random			Snowball		
		ORIGINAL SPLIT	FULL GRAPH	NO EDGES	ORIGINAL SPLIT	FULL GRAPH	NO EDGES
GCN	TRAIN ACC	0.8619 \pm 0.0103	0.7373 \pm 0.0200	0.7313 \pm 0.0127	0.9631 \pm 0.0051	0.6448 \pm 0.0085	0.7399 \pm 0.0148
	TEST ACC	0.4643 \pm 0.0224	0.5895 \pm 0.0199	0.3912 \pm 0.0123	0.4125 \pm 0.0095	0.5003 \pm 0.0188	0.3882 \pm 0.0162
GRAPH SAGE	TRAIN ACC	0.9958 \pm 0.0026	0.9663 \pm 0.0083	0.8074 \pm 0.0356	0.9998 \pm 0.0004	0.9647 \pm 0.0079	0.8308 \pm 0.0244
	TEST ACC	0.4355 \pm 0.0089	0.5243 \pm 0.0094	0.4067 \pm 0.0222	0.4030 \pm 0.0443	0.5140 \pm 0.0174	0.3907 \pm 0.0406
GAT	TRAIN ACC	0.9378 \pm 0.0203	0.6327 \pm 0.0278	0.5116 \pm 0.0111	0.9808 \pm 0.0107	0.5193 \pm 0.0230	0.4722 \pm 0.0138
	TEST ACC	0.2760 \pm 0.0388	0.4908 \pm 0.0295	0.3335 \pm 0.0210	0.3438 \pm 0.0135	0.4140 \pm 0.0295	0.3263 \pm 0.0191

TABLE VII: Train and test accuracies on PUBMED for train size 10%. Left block: random sampling; right block: snowball sampling. Values are mean \pm std when available.

Model	Metric	Random			Snowball		
		ORIGINAL SPLIT	FULL GRAPH	NO EDGES	ORIGINAL SPLIT	FULL GRAPH	NO EDGES
GCN	TRAIN ACC	0.9556 \pm 0.0049	0.8920 \pm 0.0057	0.9526 \pm 0.0032	0.9084 \pm 0.0047	0.8981 \pm 0.0075	0.8872 \pm 0.0068
	TEST ACC	0.8581 \pm 0.0029	0.8615 \pm 0.0026	0.8292 \pm 0.0044	0.8361 \pm 0.0030	0.8454 \pm 0.0018	0.8037 \pm 0.0058
GRAPHsAGE	TRAIN ACC	0.9810 \pm 0.0022	0.9364 \pm 0.0051	0.9504 \pm 0.0040	0.9944 \pm 0.0025	0.9647 \pm 0.0063	0.8178 \pm 0.0501
	TEST ACC	0.8395 \pm 0.0096	0.8401 \pm 0.0094	0.8315 \pm 0.0033	0.8026 \pm 0.0104	0.8249 \pm 0.0094	0.7240 \pm 0.0397
GAT	TRAIN ACC	0.9612 \pm 0.0038	0.8686 \pm 0.0065	0.9548 \pm 0.0018	0.9337 \pm 0.0153	0.8968 \pm 0.0055	0.8670 \pm 0.0114
	TEST ACC	0.8368 \pm 0.0031	0.8386 \pm 0.0031	0.8223 \pm 0.0051	0.8102 \pm 0.0038	0.8221 \pm 0.0016	0.7768 \pm 0.0054

TABLE VIII: Train and test accuracies on PUBMED with 50% train size. Left block: random sampling; right block: snowball sampling. Values are mean \pm std when available.

Model	Metric	Random			Snowball		
		ORIGINAL SPLIT	FULL GRAPH	NO EDGES	ORIGINAL SPLIT	FULL GRAPH	NO EDGES
GCN	TRAIN ACC	0.8924 \pm 0.0011	0.8855 \pm 0.0019	0.8887 \pm 0.0032	0.8874 \pm 0.0028	0.8885 \pm 0.0038	0.8646 \pm 0.0024
	TEST ACC	0.8696 \pm 0.0027	0.8775 \pm 0.0028	0.8624 \pm 0.0028	0.8525 \pm 0.0024	0.8715 \pm 0.0025	0.8481 \pm 0.0009
GRAPHsAGE	TRAIN ACC	0.9277 \pm 0.0018	0.9201 \pm 0.0014	0.8981 \pm 0.0016	0.9339 \pm 0.0019	0.9322 \pm 0.0011	0.8480 \pm 0.0291
	TEST ACC	0.8757 \pm 0.0017	0.8863 \pm 0.0013	0.8676 \pm 0.0014	0.8308 \pm 0.0162	0.8767 \pm 0.0027	0.8155 \pm 0.0265
GAT	TRAIN ACC	0.8881 \pm 0.0030	0.8717 \pm 0.0023	0.8855 \pm 0.0039	0.8872 \pm 0.0016	0.8870 \pm 0.0035	0.8598 \pm 0.0026
	TEST ACC	0.8610 \pm 0.0032	0.8667 \pm 0.0038	0.8581 \pm 0.0026	0.8442 \pm 0.0026	0.8582 \pm 0.0031	0.8403 \pm 0.0008

TABLE IX: Performance gap (in %) and membership advantage on CORA with train size 10%. Left block: random sampling; right block: snowball sampling.

Model	Metric	Random			Snowball		
		ORIGINAL SPLIT	FULL GRAPH	NO EDGES	ORIGINAL SPLIT	FULL GRAPH	NO EDGES
GCN	PERF. GAP	21.9735 \pm 0.7326	16.9887 \pm 0.8220	36.9408 \pm 2.0075	21.9735 \pm 0.7326	16.9887 \pm 0.8220	36.9408 \pm 2.0075
	ADV.	0.8559 \pm 0.0215	0.3387 \pm 0.0308	0.7297 \pm 0.0334	0.6908 \pm 0.0625	0.5521 \pm 0.0624	0.5287 \pm 0.0484
GRAPHsAGE	PERF. GAP	33.1583 \pm 2.0189	32.5841 \pm 2.1656	35.5202 \pm 1.5253	33.1583 \pm 2.0189	32.5841 \pm 2.1656	35.5202 \pm 1.5253
	ADV.	0.7646 \pm 0.0340	0.6808 \pm 0.0368	0.6535 \pm 0.0352	0.9330 \pm 0.0220	0.6859 \pm 0.0317	0.5715 \pm 0.0428
GAT	PERF. GAP	21.8549 \pm 1.2578	15.8714 \pm 0.9190	35.3851 \pm 2.0464	21.8549 \pm 1.2578	15.8714 \pm 0.9190	35.3851 \pm 2.0464
	ADV.	0.8494 \pm 0.0267	0.3208 \pm 0.0581	0.7096 \pm 0.0422	0.9516 \pm 0.0249	0.5313 \pm 0.0699	0.5180 \pm 0.0689

TABLE X: Performance gap (in %) and membership advantage on CORA with train size 50%. Left block: random sampling; right block: snowball sampling.

Model	Metric	Random			Snowball		
		ORIGINAL SPLIT	FULL GRAPH	NO EDGES	ORIGINAL SPLIT	FULL GRAPH	NO EDGES
GCN	PERF. GAP	19.8444 \pm 0.6248	8.3046 \pm 1.0711	24.2064 \pm 1.5491	19.8444 \pm 0.6248	8.3046 \pm 1.0711	24.2064 \pm 1.5491
	ADV.	0.3170 \pm 0.0315	0.1259 \pm 0.0262	0.2829 \pm 0.0272	0.3110 \pm 0.0423	0.3186 \pm 0.0409	0.2272 \pm 0.0232
GRAPHsAGE	PERF. GAP	21.6248 \pm 0.7822	15.0381 \pm 1.0216	23.1229 \pm 1.6155	21.6248 \pm 0.7822	15.0381 \pm 1.0216	23.1229 \pm 1.6155
	ADV.	0.5249 \pm 0.0301	0.3150 \pm 0.0339	0.2722 \pm 0.0306	0.6313 \pm 0.0403	0.4421 \pm 0.0435	0.2945 \pm 0.0262
GAT	PERF. GAP	21.9971 \pm 0.3048	9.7150 \pm 1.1748	17.9241 \pm 1.6672	21.9971 \pm 0.3048	9.7150 \pm 1.1748	17.9241 \pm 1.6672
	ADV.	0.5370 \pm 0.0315	0.1466 \pm 0.0283	0.2418 \pm 0.0277	0.5686 \pm 0.0436	0.3661 \pm 0.0393	0.2417 \pm 0.0355

TABLE XI: Performance gap (in %) and membership advantage on CHAMELEON with train size 10%. Left block: random sampling; right block: snowball sampling.

Model	Metric	Random			Snowball		
		ORIGINAL SPLIT	FULL GRAPH	NO EDGES	ORIGINAL SPLIT	FULL GRAPH	NO EDGES
GCN	PERF. GAP	60.5369 \pm 2.4519	29.2442 \pm 3.1413	60.3652 \pm 1.6069	60.5369 \pm 2.4519	29.2442 \pm 3.1413	60.3652 \pm 1.6069
	ADV.	0.8117 \pm 0.0743	0.1991 \pm 0.0498	0.6343 \pm 0.0528	0.8228 \pm 0.0326	0.3232 \pm 0.0906	0.6042 \pm 0.0616
GRAPH SAGE	PERF. GAP	67.3381 \pm 1.0025	63.0542 \pm 1.0801	63.6940 \pm 1.9714	67.3381 \pm 1.0025	63.0542 \pm 1.0801	63.6940 \pm 1.9714
	ADV.	0.9364 \pm 0.0441	0.7484 \pm 0.0703	0.6939 \pm 0.0689	0.9626 \pm 0.0231	0.7001 \pm 0.0304	0.6666 \pm 0.0556
GAT	PERF. GAP	66.0718 \pm 2.9136	29.6692 \pm 3.5059	55.8747 \pm 4.4664	66.0718 \pm 2.9136	29.6692 \pm 3.5059	55.8747 \pm 4.4664
	ADV.	0.9206 \pm 0.0493	0.1823 \pm 0.0649	0.5406 \pm 0.0516	0.9185 \pm 0.0310	0.2998 \pm 0.0727	0.4501 \pm 0.0531

TABLE XII: Performance gap (in %) and membership advantage on CHAMELEON with train size 50%. Left block: random sampling; right block: snowball sampling.

Model	Metric	Random			Snowball		
		ORIGINAL SPLIT	FULL GRAPH	NO EDGES	ORIGINAL SPLIT	FULL GRAPH	NO EDGES
GCN	PERF. GAP	46.1260 \pm 2.6407	20.0360 \pm 2.0796	46.4880 \pm 1.8716	46.1260 \pm 2.6407	20.0360 \pm 2.0796	46.4880 \pm 1.8716
	ADV.	0.5306 \pm 0.0626	0.1752 \pm 0.0328	0.3727 \pm 0.0392	0.6616 \pm 0.0268	0.3886 \pm 0.0363	0.4094 \pm 0.0374
GRAPH SAGE	PERF. GAP	56.2672 \pm 0.9544	45.7372 \pm 0.8355	49.6167 \pm 1.9626	56.2672 \pm 0.9544	45.7372 \pm 0.8355	49.6167 \pm 1.9626
	ADV.	0.8093 \pm 0.0317	0.5855 \pm 0.0368	0.4942 \pm 0.0415	0.8865 \pm 0.0368	0.5916 \pm 0.0241	0.5111 \pm 0.0470
GAT	PERF. GAP	70.5295 \pm 4.2894	22.4323 \pm 2.9691	34.7762 \pm 4.5910	70.5295 \pm 4.2894	22.4323 \pm 2.9691	34.7762 \pm 4.5910
	ADV.	0.8377 \pm 0.0340	0.1809 \pm 0.0374	0.2046 \pm 0.0402	0.7447 \pm 0.0427	0.2772 \pm 0.0320	0.2232 \pm 0.0349

TABLE XIII: Performance gap (in %) and membership advantage on PUBMED with train size 10%. Left block: random sampling; right block: snowball sampling.

Model	Metric	Random			Snowball		
		ORIGINAL SPLIT	FULL GRAPH	NO EDGES	ORIGINAL SPLIT	FULL GRAPH	NO EDGES
GCN	PERF. GAP	10.1968 \pm 0.5254	3.4195 \pm 0.5979	12.9579 \pm 0.5070	10.1968 \pm 0.5254	3.4195 \pm 0.5979	12.9579 \pm 0.5070
	ADV.	0.3962 \pm 0.0311	0.0530 \pm 0.0104	0.1553 \pm 0.0147	0.2910 \pm 0.0728	0.3720 \pm 0.0517	0.1845 \pm 0.0575
GRAPH SAGE	PERF. GAP	14.4283 \pm 0.8529	10.2852 \pm 0.7891	12.5104 \pm 0.3285	14.4283 \pm 0.8529	10.2852 \pm 0.7891	12.5104 \pm 0.3285
	ADV.	0.2554 \pm 0.0376	0.1221 \pm 0.0150	0.1549 \pm 0.0198	0.3416 \pm 0.0506	0.2488 \pm 0.0573	0.1943 \pm 0.0381
GAT	PERF. GAP	12.9438 \pm 0.3823	3.4487 \pm 0.6849	13.8838 \pm 0.4137	12.9438 \pm 0.3823	3.4487 \pm 0.6849	13.8838 \pm 0.4137
	ADV.	0.2036 \pm 0.0297	0.0547 \pm 0.0127	0.1690 \pm 0.0168	0.2635 \pm 0.0649	0.2224 \pm 0.0718	0.1768 \pm 0.0623

TABLE XIV: Performance gap (in %) and membership advantage on PUBMED with train size 50%. Left block: random sampling; right block: snowball sampling.

Model	Metric	Random			Snowball		
		ORIGINAL SPLIT	FULL GRAPH	NO EDGES	ORIGINAL SPLIT	FULL GRAPH	NO EDGES
GCN	PERF. GAP	2.5561 \pm 0.2790	0.9029 \pm 0.4466	2.9609 \pm 0.3387	2.5561 \pm 0.2790	0.9029 \pm 0.4466	2.9609 \pm 0.3387
	ADV.	0.0448 \pm 0.0109	0.0180 \pm 0.0089	0.0400 \pm 0.0093	0.2066 \pm 0.0168	0.3206 \pm 0.0130	0.0647 \pm 0.0108
GRAPH SAGE	PERF. GAP	5.5948 \pm 0.3011	3.6743 \pm 0.2266	3.3914 \pm 0.2173	5.5948 \pm 0.3011	3.6743 \pm 0.2266	3.3914 \pm 0.2173
	ADV.	0.0697 \pm 0.0106	0.0531 \pm 0.0139	0.0465 \pm 0.0119	0.4324 \pm 0.0134	0.0890 \pm 0.0132	0.0599 \pm 0.0144
GAT	PERF. GAP	3.0500 \pm 0.3526	0.5754 \pm 0.4008	3.0906 \pm 0.2589	3.0500 \pm 0.3526	0.5754 \pm 0.4008	3.0906 \pm 0.2589
	ADV.	0.0611 \pm 0.0108	0.0229 \pm 0.0121	0.0436 \pm 0.0111	0.2172 \pm 0.0153	0.0910 \pm 0.0172	0.0598 \pm 0.0100